Giant tunneling electroresistance in two-dimensional ferroelectric tunnel junctions with out-of-plane ferroelectric polarization

Lili Kang,[1,2,3] Peng Jiang,[1,3] Hua Hao,[1] Yanhong Zhou,[4] Xiaohong Zheng,[1,2,3,4,*] Lei Zhang,[2,5,†] and Zhi Zeng[1,3]

[1]*Key Laboratory of Materials Physics, Institute of Solid State Physics, Chinese Academy of Sciences, Hefei 230031, China*

[2]*State Key Laboratory of Quantum Optics and Quantum Optics Devices, Institute of Laser Spectroscopy, Shanxi University, Taiyuan 030006, China*

[3]*University of Science and Technology of China, Hefei 230026, China*

[4]*College of Science, East China Jiao Tong University, Nanchang, Jiangxi 330013, China*

[5]*Collaborative Innovation Center of Extreme Optics, Shanxi University, Taiyuan 030006, China*

(Received 24 October 2019; revised manuscript received 8 December 2019; published 14 January 2020)

Ferroelectric tunnel junctions (FTJs) have been intensively studied in recent years due to the great potential in nonvolatile memory devices and two-dimensional (2D) FTJs have started to catch attention lately because of their atomic thickness and their significance in miniaturizing FTJ device sizes. In this work, we propose a mechanism for building 2D FTJs based on the large difference between the two work functions of a 2D ferroelectric polar material with out-of-plane polarization. When it forms a van der Waals (vdW) vertical heterostructure with another 2D material there will be two kinds of interfaces, according to which surface of the 2D polar material is contacted. Depending on the relative work functions of the contacted surfaces of the two materials, charge transfer may or may not occur between them, thus the 2D polar material may become conducting or be still insulating, resulting in two distinct conducting states ("ON" and "OFF"). We demonstrate the feasibility of this proposal by the example of a vdW heterostructure FTJ constructed with graphene and 2D ferroelectric In_2Se_3 with out-of-plane polarization. Specifically, based on density functional calculations, we show that excellent tunnel electroresistance (TER) effect with TER ratio $\sim 1 \times 10^8\%$ is achieved, suggesting a promising route for applying 2D ferroelectric materials with out-of-plane polarization in ferroelectric memory devices.

DOI: 10.1103/PhysRevB.101.014105

I. INTRODUCTION

Ferroelectric tunnel junctions (FTJs), which use ferroelectric materials as the central tunnel barrier and metal or semiconductor as leads, have been widely studied in both experiments and theory due to their potential applications in nonvolatile memory devices [1–3]. The tunnel electroresistance (TER) ratio is a very important parameter characterizing the performance of data storage in the study of FTJs [4,5]. Thus far, there have been numerous studies about how to design high-performance FTJs with a very large TER ratio [6–9]. However, most of the attention has been paid to FTJs adopting thin films of three-dimensional (3D) ferroelectric materials as the tunnel barrier [10–13], and the most common ferroelectric materials adopted are perovskite-type oxide materials, such as $BaTiO_3$ and $PbTiO_4$, etc. [14–17]. It is well known that there is a limit in critical thickness of 3D ferroelectric materials for the observation of spontaneous polarization because of the charge accumulation on the surfaces, which is in contradiction with requirements in the device miniaturization [18,19]. Thus, how to decrease the critical thickness of the ferroelectric thin films is a key problem in the further development of high-performance FTJs.

An emerging direction in the study of ferroelectric materials these years is the search of two-dimensional (2D) ferroelectric materials and many of them with either in-plane or out-of-plane spontaneous polarization have been predicted by theory [20–25] and even prepared in experiments [26]. 2D materials provide a natural good candidate for construction of devices with atomic thickness. If 2D ferroelectric materials can be adopted to construct high-performance FTJs with a large TER ratio, it will greatly reduce the thickness of the FTJ device. As a matter of fact, the application of 2D ferroelectric materials in FTJs has already started to catch research attention lately. In one of our recent studies of 2D FTJ constructed by ferroelectric BiP with in-plane polarization, a TER of 623% is achieved by differentiating the leads with hole and electron doping, respectively [27]. Duan *et al.* revealed a giant TER effect of 1460% in the In:SnSe/SnSe/Sb:SnSe system with in-plane ferroelectric polarization based on the dynamical modulation of both barrier width and barrier height during the ferroelectric switching [28]. In these studies, the TER effect is implemented as usual through breaking the symmetry of the left and right leads, so that asymmetric screening lengths in the two leads are achieved, which is the basis of the earliest proposed and the most well-known TER mechanism [29]. Shen *et al.* proposed a special kind of in-plane FTJ with a 2D ferroelectric layer together with another insulating layer as the tunnel barrier and finite cross section in size by making use of upward or downward band bending in the ferroelectric

*xhzheng@theory.issp.ac.cn
†zhanglei@sxu.edu.cn

layer, where the band bending is brought by the ferroelectric polarization and tunable by the ferroelectric switching. The band bending leads to metal-insulator transition in the edge region of the ferroelectric layer, which changes the tunnel barrier width and leads to a large TER [30].

We intend to propose a mechanism for building 2D FTJs based on the two different work functions that each 2D insulating polar material has on its two surfaces. When it forms a van der Waals (vdW) vertical heterostructure with another 2D material that has a work function close to one of its work functions, there will be two kinds of interfaces, depending on which surface of the 2D polar material is contacted. In the case where the contacted surfaces of the two materials have close work functions, there will be no charge transfer between them and the 2D polar material will be kept insulating. In contrast, in the other case where the two contacted surfaces have greatly different work functions, charge transfer between them leads to the partial filling of the original full valence band or empty conduction band of the 2D polar material and thus an insulator-metal transition may occur. 2D ferroelectric materials with out-of-plane ferroelectric polarization are a kind of such 2D polar materials and the charge-transfer induced conducting state change may well be utilized to build 2D FTJs.

In this work, we will demonstrate that α-In_2Se_3, a 2D material with both in-plane and out-of-plane ferroelectric polarizations that has attracted great attention recently [31–35], serves as an excellent exemplary material for building a vdW FTJ with a very large TER ratio based on our proposal. Previously, it has been shown that, by using a α-In_2Se_3 layer, a switchable room-temperature ferroelectric double diode is built [35], with a pronounced on/off ratio of 1×10^5 and a 2D ferroelectric field-effect transistor (FeFET) is realized [34], which indicates that 2D α-In_2Se_3 holds great potential for building nanoscale logic devices. Here, specifically, we design a 2D out-of-plane ferroelectric tunnel junction adopting the graphene/In_2Se_3 vdW vertical heterostructure as left/right lead and In_2Se_3 as the central ferroelectric tunneling barrier. By density functional calculations combined with a nonequilibrium Green's function technique, we obtain a giant TER ratio of around 1×10^8%, which is higher than that of most current 3D FTJs.

II. STRUCTURE AND COMPUTATION DETAILS

As shown in Fig. 1, the vdW graphene/In_2Se_3 FTJ is composed of three parts: left lead (L), right lead (R), and the central scattering region (C). The left/right leads are both graphene/In_2Se_3 vdW vertical heterostructure and the transport channel is the monolayer In_2Se_3. Figures 1(a) and 1(b) show the two cases with the directions of polarization of In_2Se_3 pointing upward ($P_\uparrow$) and downward ($P_\downarrow$), respectively. The system in the direction of the x axis is periodic and the transport direction is along the z axis. Figures 1(c) and 1(d) are the top views of the lead supercell for the $P_\uparrow$ and $P_\downarrow$ cases. The size of a rectangular unit cell of graphene is 2.46 Å × 4.26 Å and that of In_2Se_3 is 7.11 Å × 4.106 Å. Therefore, we choose 3×1 graphene unit cells and 1×1 In_2Se_3 unit cell to build the lead supercell. In this way, the lattice mismatch is only about 3.6% along the directions of both x and z axes. In the

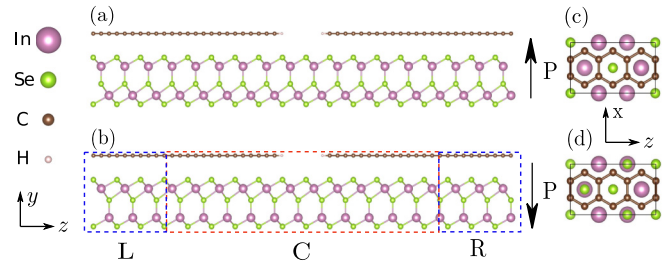

FIG. 1. The structure of the FTJ with (a) upward polarization and (b) downward polarization. The structure is divided into three parts: left (L) and right (R) leads, and the central scattering region (C). The left/right leads are graphene/In_2Se_3 vdW vertical heterostructure. The channel is 2D In_2Se_3. Panels (c) and (d) are the top views of the lead for upward and downward polarizations, respectively.

numerical simulation, we keep the ferroelectric properties of the In_2Se_3 layer unaffected; only the lattice constants of graphene are slightly stretched and compressed along the armchair and zigzag directions, respectively. In the y direction, a vacuum space with thickness of 30 Å is chosen to avoid interaction between adjacent neighbors.

The geometry relaxation is performed by the Vienna Ab initio Simulation Package (VASP), [36,37] which is based on density functional theory (DFT) using the projector-augmented wave method and a plane-wave basis set [38]. The generalized gradient approximation (GGA) with a form of Perdew-Burke-Ernzerhof (PBE) [39] is adopted for the exchange-correlation potential. The energy cutoff is set to be 500 eV. In the atomic structure relaxation, the vdW interaction is taken into consideration by the DFT-D3 method. The k-point sampling grid is chosen as $8 \times 1 \times 5$. The structures are deemed fully relaxed when the Hellmann-Feynman force tolerance gets below 1 meV/Å and the electronic energy difference between two consecutive steps gets below 10^{-6} eV. The interlayer spacings between graphene and In_2Se_3 are finally relaxed as 3.51 and 3.53 Å for the $P_\uparrow$ and $P_\downarrow$ cases, respectively. Accompanying with the ferroelectric switching from $P_\uparrow$ to $P_\downarrow$, the atomic geometry of the In_2Se_3 changes only a little. For example, its thickness slightly changes from 6.760 to 6.749 Å, while the polarization changes from $P = 0.112e$· Å/unit cell to $0.012e$ Å/unit cell, as compared with $P = 0.094e$ Å/unit cell of the pristine In_2Se_3.

The calculations for electronic structure and quantum transport are performed by the TranSIESTA method [40,41], which combines the density functional theory (DFT) and the nonequilibrium Green's function (NEGF) technique for the study of open systems and is included in the SIESTA package [42,43]. The generalized gradient approximation (GGA) with a form of Perdew-Burke-Ernzerhof (PBE) [39] is applied for the exchange-correlation potential. The cutoff energy is set to be 250 Ry in our case. The basis type is double zeta basis plus polarization (DZP) and the k-point mesh is chosen as $10 \times 1 \times 1$ for the self-consistent (SC) calculation of the central scattering region. For transmission calculation, the TBTrans code is used and the k-point mesh is chosen as $1000 \times 1 \times 1$ because the k-point number needs to be much larger for convergence. The tunnel equilibrium conductance is

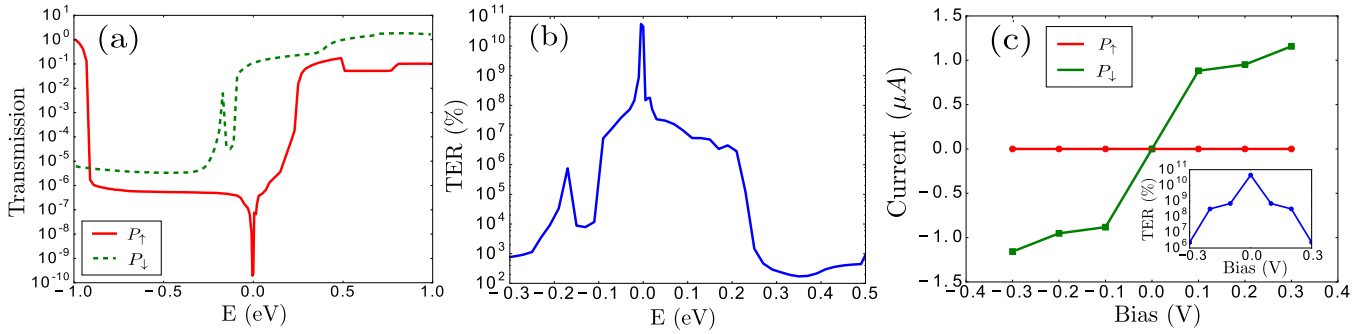

FIG. 2. The transmission function for both polarization directions, with the Fermi level set to 0 eV; (b) the TER ratio as a function of electron energy; (c) the *I-V* curves for both polarization directions, with the inset showing the TER at low bias.

obtained by the formula

$$G = \frac{2e^2}{h} \sum_{k_{||}} T(k_{||}, E = E_F, V = 0) \tag{1}$$

and the current by

$$I = \frac{2e^2}{h} \int dE T(E, V)[f_L(E) - f_R(E)], \tag{2}$$

where $T(k_{||}, E, V)$ is the transmission function at energy E and bias V with $k_{||} = k_x$. $T(E, V)$ is the k-point averaged transmission function at energy E and bias V. $f_\alpha(E)(\alpha = L, R)$ is the Fermi distribution of electrons in the left or right lead. E_F is the lead Fermi energy. e and h are the electron charge and Plank's constant, respectively. The TER ratio is defined as [10]

$$\text{TER} = \frac{|G_\uparrow - G_\downarrow|}{\min(G_\uparrow, G_\downarrow)} \tag{3}$$

at equilibrium and

$$\text{TER} = \frac{|I_\uparrow - I_\downarrow|}{\min(I_\uparrow, I_\downarrow)} \tag{4}$$

at finite bias, where $G_\uparrow(I_\uparrow)$ and $G_\downarrow(I_\downarrow)$ are the tunnel equilibrium conductances (current at finite bias) of the FTJ in the $P_\uparrow$ and $P_\downarrow$ cases, respectively. Since the system's Fermi level is a reference point that can be shifted through a gate placed on the whole device, although the equilibrium TER ratio is defined by the tunnel equilibrium conductance as determined by the transmission function at E_F, it can be extended to any other energy E based on the equilibrium transmission function to give a rough estimation of TER ratio at that energy. Note that since there is out-of-plane polarization in the 2D In_2Se_3 slab, for the sake of accuracy, the dipole correction [44] has been taken into consideration in all our calculations.

III. RESULTS AND DISCUSSION

First of all, the transmission functions at zero bias for both polarization directions are presented in Fig. 2(a). It is found that, around the Fermi level, the transmission in the $P_\downarrow$ case is a few orders of magnitude larger than that in the $P_\uparrow$ case. Especially, for the $P_\uparrow$ case, there is a sharp dip in the transmission function at the Fermi level. With the transmission function, we can get the tunnel equilibrium conductance by Eq. (1) and further the TER ratio by Eq. (3). The extended TER as a function of energy is shown in Fig. 2(b), from which we see that the maximum TER ratio reaches the order of $1.0 \times 10^{10}\%$ at the Fermi level, which is a few orders of magnitude larger than those previously reported [14,45,46]. Even away from E_F, the TER ratio is still very high, although it gets smaller than that at the Fermi level. Near the Fermi level, the TER is always larger than $1 \times 10^7\%$, which indicates that very large TER will still be achieved at low bias. To prove this, Fig. 3(c) shows the *I-V* characteristics for both polarization directions and the TER at low bias. The bias effect on the electronic structure and transmission function of the system has been self-consistently considered. It is seen that the *I-V* curve is symmetric with respect to the polarity of bias as expected from the symmetric structure of our FTJ. The most notable feature is that there is a distinct magnitude difference between the currents $I_\uparrow$ in the $P_\uparrow$ case and $I_\downarrow$ in the $P_\downarrow$ case. The TER is always larger than $1 \times 10^6\%$. Especially at $V = 0.1$ and 0.2 V, the TER is larger than $1 \times 10^8\%$, displaying two ideal "0" and "1" states for data storage.

In order to understand the origin of the giant TER ratio observed above, we analyze the electronic structure of the FTJ, and the local density of states (LDOS) distribution of the central scattering region as a function of the energy E and position z is shown in Figs. 3(a) and 3(b) for the $P_\uparrow$ and $P_\downarrow$ cases, respectively. It is averaged over the xy plane. The black dotted box indicates the transport channel region. It is found that there are almost no electronic states in the transport channel around the Fermi level in the $P_\uparrow$ case, which is in clear contrast to the $P_\downarrow$ case where we can see a large LDOS distribution. Thus, the $P_\downarrow$ case conducts much better than the $P_\uparrow$ case, consistent with the marked difference in the tunnel equilibrium conductance and current as shown above. Further analysis indicates that the electronic states in the transport channel in the $P_\downarrow$ case are contributed by the In_2Se_3 layer. Figures 3(c) and 3(d) show the LDOS of the In_2Se_3 layer extracted from the total LDOS of the FTJ in the $P_\uparrow$ and $P_\downarrow$ cases, respectively. It is clear that the gap between the conduction-band minimum (CBM) and the valence-band maximum (VBM) is in the energy range of around $E = -0.8$ to 0.2 eV for the $P_\uparrow$ case while that for the $P_\downarrow$ case is around $E = -1.2$ to -0.2 eV. As a result, the Fermi level is right inside the gap for the $P_\uparrow$ case and that for the $P_\downarrow$ case is in the conduction band. That is why in Fig. 3(b), finite density of states is observed around the Fermi level in the $P_\downarrow$ case.

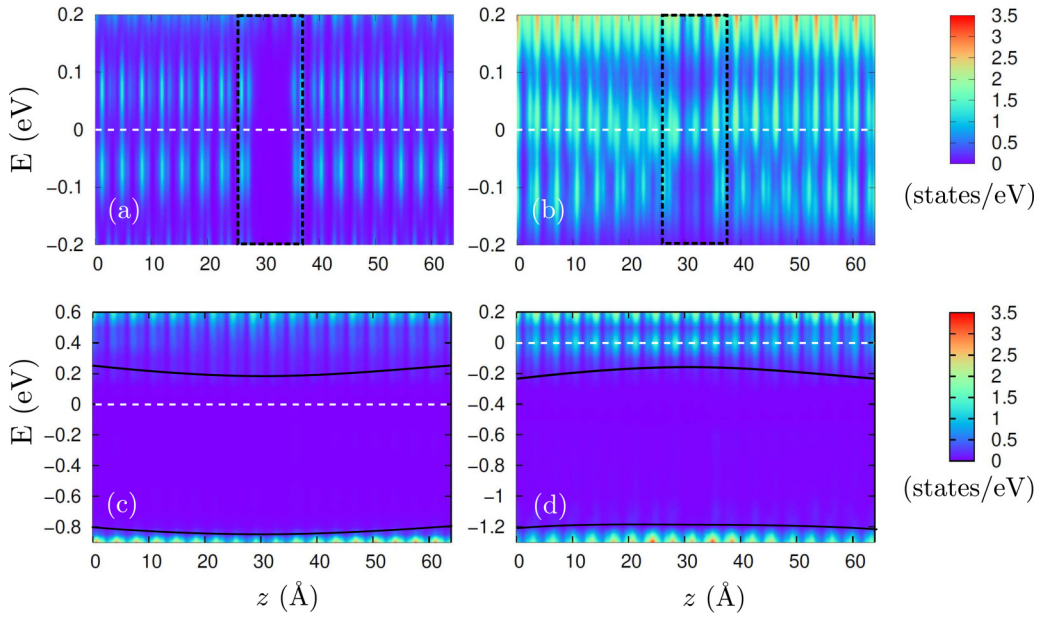

FIG. 3. The averaged LDOS distribution over the *xy* plane of the central scattering regions as a function of electron energy E and position z for (a) $P_\uparrow$ and (b) $P_\downarrow$ and the corresponding LDOS contribution of the In_2Se_3 layer extracted from the total LDOS: (c) $P_\uparrow$ and (d) $P_\downarrow$. The black dotted box represents the transport channel region. The white dashed lines indicate the Fermi level and the black solid curves indicate the CBM and the VBM of the In_2Se_3 layer.

Obviously, it is the reverse of the ferroelectric polarization that results in the different Fermi-level positions in the $P_\uparrow$ and $P_\downarrow$ cases. To have a deeper insight, we have investigated the electronic structure of bulk systems of graphene/In_2Se_3 for the $P_\uparrow$ and $P_\downarrow$ cases. The layer-resolved band structures are shown in Fig. 4. First, since the vdW interaction between graphene and In_2Se_3 is weak, basically no hybridization between the layers is observed and thus the band structures of the two layers are well separated. Second, for the $P_\uparrow$ case shown in Fig. 4(a) the Dirac point of graphene is observable at the Γ point and almost not affected by the In_2Se_3 layer. Meanwhile, the In_2Se_3 layer still remains semiconducting, which indicates that the charge transfer between the graphene layer and the $P_\uparrow$ polarized In_2Se_3 layer is negligible. In contrast, for the $P_\downarrow$ case shown in Fig. 4(b), one band contributed by the In_2Se_3 layer crosses the Fermi level and the Dirac point of the graphene layer gets slightly above the Fermi level, which indicates that the In_2Se_3 layer receives electrons from the graphene layer and it becomes conducting.

In the following, we will understand why there are two forms of contact with different charge transfer in the $P_\uparrow$ and $P_\downarrow$ cases. It is well known that, in a 2D ferroelectric material with out-of-plane polarization, the symmetry in the vertical direction is broken, which leads to the different work functions at the two sides of the material. The effective potential along the vertical (y) direction of In_2Se_3 and graphene is shown in Fig. 5, where we find that the effective potentials of the "up" side and the "dn" (down) side of In_2Se_3 differ by 2.396 eV. As a contrast, the effective potentials of the two sides of graphene are equal, which is consistent with the property of 2D nonpolar materials. The work function is defined as

$$W = E_0 - E_F, \tag{5}$$

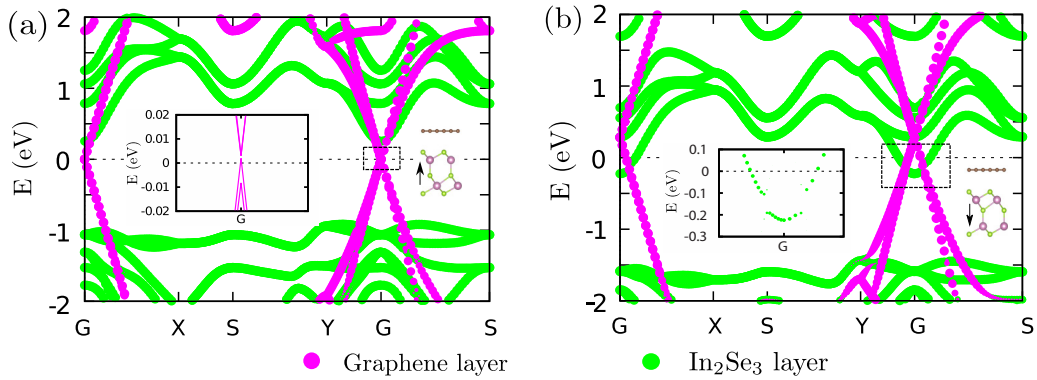

FIG. 4. The layer-resolved band structure of graphene/In_2Se_3 vdW heterostructure for (a) $P_\uparrow$ and (b) $P_\downarrow$. The insets show the locally magnified region indicated by the dashed line box around the G point.

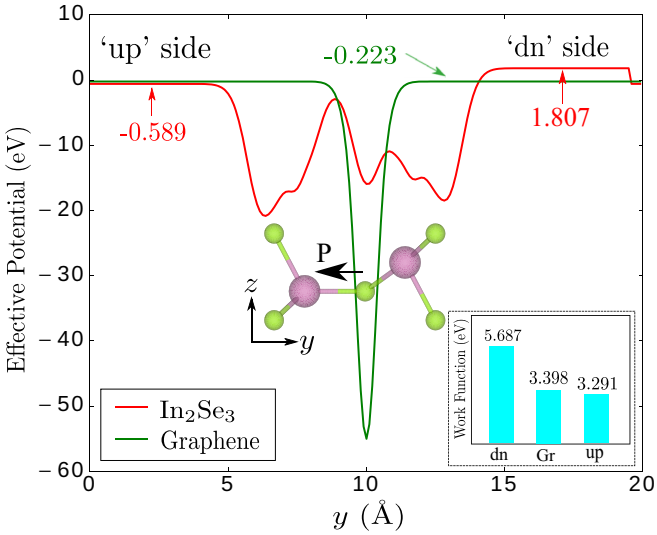

FIG. 5. The effective potential along the y direction (the direction of vacuum layer) of In_2Se_3 (red solid line) and graphene (green solid line). The "up" side and "dn" side marked on the figure are the two sides of In_2Se_3. The black arrow is the polarization direction of In_2Se_3. The inset indicates the work functions of graphene, "up" side and "dn" side of In_2Se_3.

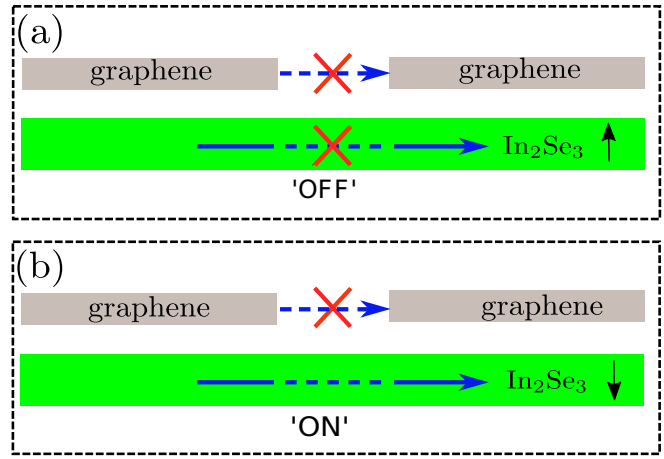

FIG. 6. The schematic diagram of transport process for the case: (a) $P_\uparrow$ and (b) $P_\downarrow$. The blue arrows show the possible transmission channels and the red cross means the blocking of the corresponding transmission channel.

where E_F is the Fermi level and E_0 is the vacuum level, corresponding to the effective potential at the vacuum layer in our calculations. By Eq. (4), we obtain the work functions of graphene (W_{Gr}), "up" side (W_{up}) and "dn" side (W_{dn}) of In_2Se_3 as 3.398, 3.291, and 5.687 eV, which are shown in the inset of Fig. 5. It is well known that electrons will flow from the lower work-function side to the other when two different materials are in contact until their Fermi levels become equal [47]. Therefore, with the relation of $W_{up} < W_{Gr} < W_{dn}$, when the graphene layer contacts with the "up" side of In_2Se_3 (the $P_\uparrow$ case), there will be negligible electron transfer between In_2Se_3 and graphene due to the little difference between W_{Gr} and W_{up}. On the contrary, when graphene contacts with the "dn" side of In_2Se_3 (the $P_\downarrow$ case), considerable electrons will flow from graphene to In_2Se_3 due to the much smaller W_{Gr} than W_{dn}, thus both graphene and In_2Se_3 become conducting. This is exactly what we have obtained previously in the discussion of the band structures shown in Figs. 4(a) and 4(b). It is unambiguously supported by Mulliken population analysis: we obtain zero charge transfer in the $P_\uparrow$ case and 0.13 electrons per unit cell transferred from the graphene layer to the In_2Se_3 layers in the $P_\downarrow$ case, consistent with the band structure in Fig. 4.

Now, we give a physical picture for why the TER ratio is so large by a simple schematic diagram of transport process as shown in Fig. 6. The transport path of electrons through the graphene/In_2Se_3 FTJ can be divided into two channels, which are the graphene layer and the In_2Se_3 layer. It is seen obviously that the channel contributed by the graphene layer through the vacuum is blocked for both the $P_\uparrow$ case and the $P_\downarrow$ case due to the real-space gap in the middle. In addition, according to the previous discussion, we know that the In_2Se_3 layer in the $P_\uparrow$ case is still a semiconductor, which means that the channel contributed by In_2Se_3 is also blocked since there are no states in the In_2Se_3 layer of either the leads or the channel region. Therefore, almost no electrons go through the FTJ in the $P_\uparrow$ case, which leads to the "OFF" or "0" state with low transmission coefficient. In contrast, for the $P_\downarrow$ case, the In_2Se_3 layer in the leads is metallic. As a result, electrons can transport through the In_2Se_3 layer through a tunneling mechanism with a considerably high transmission, which leads to the "ON" or "1" state with high transmission coefficient. The role of the graphene layer lies in the donation or no donation of electrons to the In_2Se_3 layer, depending on the relative change of work functions of In_2Se_3 as triggered by the reverse of its polarization by an external electric field.

Finally, we reserve a special discussion for the sharp dip observed at the Fermi level in the equilibrium transmission function in the $P_\uparrow$ case but not in the $P_\downarrow$ case, which is obviously beneficial for achieving a large TER ratio. We find that such a sharp dip is due to the minigap in the band structure of graphene induced by strain or stress [see the inset in Fig. 4(a)]. In our calculations, to get the same lattice constants for the graphene and In_2Se_3 layers, the graphene layer is artificially slightly stretched or compressed. It has been reported that strain or stress will lead to a minigap in graphene [48,49]. Although such a strain or stress is introduced "artificially" due to calculation reasons, in real situations, strain or stress is very common when two different materials are grown together [50,51]. Thus, such a stress or strain induced minigap can even be well utilized intentionally to achieve a large TER ratio in the design of 2D FTJs. In addition, the minigap induced sharp dip becomes apparent only in the $P_\uparrow$ case where both transport channels are negligible as shown in Fig. 6. It does not show up in the $P_\downarrow$ case since it is masked by the large transmission of the transport channel through the In_2Se_3 layer. Of course, a very large TER ratio can be achieved in a large energy range around the Fermi level. Even without the contribution from the minigap in graphene, we can still get a very large TER (order of $\sim 1 \times 10^8\%$) in current under finite bias, as shown previously. Furthermore, another dip to note is the one at $E = -0.13$ eV in the equilibrium transmission function of the

$P_\downarrow$ case [see Fig. 2(a)], which obviously leads to the dip at the same energy in the TER curve in Fig. 2(b). This dip is found to arise from a minigap in the layer-resolved band structure [as indicated by the inset in Fig. 4(b)] of In_2Se_3 due to the interaction between graphene and In_2Se_3.

IV. CONCLUSION

In conclusion, we have proposed a type of 2D vdW FTJs constructed by 2D ferroelectric material with out-of-plane ferroelectric polarization. Our proposal works on the change of the conducting states (metallic or insulating) of the 2D ferroelectric material itself with the change of work function and charge transfer which are tunable by an external electric field. It is in clear contrast with the general schemes where asymmetric structures characterized either by different leads or by different interfaces between the leads and the tunnel barrier to tune the tunnel barrier height or barrier width are required. Since our mechanism is based on the change between the metallic and insulating nature of the 2D ferroelectric material, an extremely high TER ratio can be easily achieved. As an example, we adopt the 2D ferroelectric material In_2Se_3 with out-of-plane ferroelectric polarization as the central tunneling barrier and graphene/In_2Se_3 vdW vertical heterostructure as the left/right leads to build a vdW 2D FTJ, in which we obtain a giant TER ratio of around $1 \times 10^8\%$. By electronic structure calculations, we show that the In_2Se_3 layer of graphene/In_2Se_3 vdW vertical heterostructure still remains semiconducting in the $P_\uparrow$ case while it is metallic in the $P_\downarrow$ case. Further analysis indicates that the different conducting states of In_2Se_3 in graphene/In_2Se_3 vdW structure arise from the big difference ($\sim$2.396 eV) in work functions of the two surfaces of the In_2Se_3 slab, which leads to different charge transfer from graphene to In_2Se_3 and different electron filling of the bands of In_2Se_3 around the Fermi level when it contacts with graphene. Our proposal is general and can be conveniently utilized to design high-performance 2D FTJs based on any 2D ferroelectric material with out-of-plane ferroelectric polarization by taking only work functions as the major consideration.

ACKNOWLEDGMENT

We gratefully acknowledge financial support by the National Natural Science Foundation of China under Grants No. 11974355 (X.Z.), No. 11574318 (X.Z.), and No. 11704232 (L.Z.); Shanxi Science and Technology Department (Grant No. 201701D121003) (L.Z.) and the Program of State Key Laboratory of Quantum Optics and Quantum Optics Devices (Grant No. KF201810) (X.Z. and L.Z.); National Key R&D Program of China under Grant No. 2017YFA0304203 (L.Z.); and Shanxi Province 100-Plan Talent Program (L.Z.). Calculations were performed in the Center for Computational Science of CASHIPS, the ScGrid of Supercomputing Center and Computer Network Information Center of Chinese Academy of Sciences.

[1] R. C. Naber, K. Asadi, P. W. Blom, D. M. de Leeuw, and B. de Boer, Adv. Mater. **22**, 933 (2010).
[2] J. T. Evans and R. Womack, IEEE J. Solid-State Circuits **23**, 1171 (1988).
[3] O. Auciello, J. F. Scott, and R. Ramesh, Phys. Today **51**(7), 22 (1998).
[4] V. Garcia, S. Fusil, K. Bouzehouane, S. Enouz-Vedrenne, N. D. Mathur, A. Barthelemy, and M. Bibes, Nature (London) **460**, 81 (2009).
[5] V. Garcia and M. Bibes, Nat. Commun. **5**, 4289 (2014).
[6] A. Gruverman, D. Wu, H. Lu, Y. Wang, H. Jang, C. Folkman, M. Y. Zhuravlev, D. Felker, M. Rzchowski, C.-B. Eom *et al.*, Nano Lett. **9**, 3539 (2009).
[7] C. Li, L. Huang, T. Li, W. Lü, X. Qiu, Z. Huang, Z. Liu, S. Zeng, R. Guo, Y. Zhao *et al.*, Nano Lett. **15**, 2568 (2015).
[8] D. Wortmann and S. Blügel, Phys. Rev. B **83**, 155114 (2011).
[9] A. Crassous, V. Garcia, K. Bouzehouane, S. Fusil, A. Vlooswijk, G. Rispens, B. Noheda, M. Bibes, and A. Barthélémy, Appl. Phys. Lett. **96**, 042901 (2010).
[10] L. Tao and J. Wang, Appl. Phys. Lett. **108**, 062903 (2016).
[11] K. Klyukin, L. L. Tao, E. Y. Tsymbal, and V. Alexandrov, Phys. Rev. Lett. **121**, 056601 (2018).
[12] P.-Z. Wang, T.-Y. Cai, S. Ju, and Y.-Z. Wu, Sci. Rep. **6**, 24209 (2016).
[13] Z. Wen, C. Li, D. Wu, A. Li, and N. Ming, Nat. Mater. **12**, 617 (2013).
[14] R. Soni, A. Petraru, P. Meuffels, O. Vavra, M. Ziegler, S. K. Kim, D. S. Jeong, N. A. Pertsev, and H. Kohlstedt, Nat. Commun. **5**, 5414 (2014).
[15] H. Lu, A. Lipatov, S. Ryu, D. Kim, H. Lee, M. Y. Zhuravlev, C.-B. Eom, E. Y. Tsymbal, A. Sinitskii, and A. Gruverman, Nat. Commun. **5**, 5518 (2014).
[16] V. S. Borisov, S. Ostanin, S. Achilles, J. Henk, and I. Mertig, Phys. Rev. B **92**, 075137 (2015).
[17] D. I. Bilc, F. D. Novaes, J. Íñiguez, P. Ordejón, and P. Ghosez, ACS Nano **6**, 1473 (2012).
[18] J. Junquera and P. Ghosez, Nature (London) **422**, 506 (2003).
[19] D. Fong, Science **304**, 1650 (2004).
[20] F. Xiong, X. Zhang, Z. Lin, and Y. Chen, J. Materiomics **4**, 139 (2018).
[21] A. I. Lebedev, J. Appl. Phys. **124**, 164302 (2018).
[22] R. Fei, W. Kang, and L. Yang, Phys. Rev. Lett. **117**, 097601 (2016).
[23] C. Xiao, F. Wang, S. A. Yang, Y. Lu, Y. Feng, and S. Zhang, Adv. Funct. Mater. **28**, 1707383 (2018).
[24] C. Liu, W. Wan, J. Ma, W. Guo, and Y. Yao, Nanoscale **10**, 7984 (2018).
[25] K. Chang, J. Liu, H. Lin, N. Wang, K. Zhao, A. Zhang, F. Jin, Y. Zhong, X. Hu, and W. Duan, Science **353**, 274 (2016).
[26] C. Cui, W.-J. Hu, X. Yan, C. Addiego, W. Gao, Y. Wang, Z. Wang, L. Li, Y. Cheng, P. Li *et al.*, Nano Lett. **18**, 1253 (2018).
[27] L. Kang, P. Jiang, N. Cao, H. Hao, X. Zheng, L. Zhang, and Z. Zeng, Nanoscale **11**, 16837 (2019).
[28] X. Shen, Y.-W. Fang, B. Tian, and C.-G. Duan, ACS Appl. Electron. Mater. **1**, 1133 (2019).
[29] M. Y. Zhuravlev, R. F. Sabirianov, S. S. Jaswal, and E. Y. Tsymbal, Phys. Rev. Lett. **94**, 246802 (2005).

[30] H. Shen, J. Liu, K. Chang, and L. Fu, Phys. Rev. Appl. **11**, 024048 (2019).
[31] W. Ding, J. Zhu, Z. Wang, Y. Gao, D. Xiao, Y. Gu, Z. Zhang, and W. Zhu, Nat. Commun. **8**, 14956 (2017).
[32] T. Ayadi, L. Debbichi, M. Badawi, M. Said, H. Kim, D. Rocca, and S. Lebègue, Physica E (Amsterdam, Neth.) **114**, 113582 (2019).
[33] F. Zhang, Z. Wang, J. Dong, A. Nie, J. Xiang, W. Zhu, Z. Liu, and C. Tao, ACS Nano **13**, 8004 (2019).
[34] S. Wan, Y. Li, W. Li, X. Mao, C. Wang, C. Chen, J. Dong, A. Nie, J. Xiang, Z. Liu *et al.*, Adv. Funct. Mater. **29**, 1808606 (2019).
[35] S. Wan, Y. Li, W. Li, X. Mao, W. Zhu, and H. Zeng, Nanoscale **10**, 14885 (2018).
[36] G. Kresse and J. Furthmüller, Phys. Rev. B **54**, 11169 (1996).
[37] G. Kresse and D. Joubert, Phys. Rev. B **59**, 1758 (1999).
[38] P. E. Blöchl, Phys. Rev. B **50**, 17953 (1994).
[39] J. P. Perdew, K. Burke, and M. Ernzerhof, Phys. Rev. Lett. **77**, 3865 (1996).
[40] M. Brandbyge, J.-L. Mozos, P. Ordejón, J. Taylor, and K. Stokbro, Phys. Rev. B **65**, 165401 (2002).
[41] N. Papior, N. Lorente, T. Frederiksen, A. García, and M. Brandbyge, Comput. Phys. Commun. **212**, 8 (2017).
[42] D. Sánchez-Portal, P. Ordejon, E. Artacho, and J. M. Soler, Int. J. Quantum Chem. **65**, 453 (1997).
[43] J. M. Soler, E. Artacho, J. D. Gale, A. García, J. Junquera, P. Ordejón, and D. Sánchez-Portal, J. Phys.: Condens. Matter **14**, 2745 (2002).
[44] L. Bengtsson, Phys. Rev. B **59**, 12301 (1999).
[45] A. Zenkevich, M. Minnekaev, Y. Matveyev, Y. Lebedinskii, K. Bulakh, A. Chouprik, A. Baturin, K. Maksimova, S. Thiess, and W. Drube, Appl. Phys. Lett. **102**, 062907 (2013).
[46] Z. Li, X. Guo, H.-B. Lu, Z. Zhang, D. Song, S. Cheng, M. Bosman, J. Zhu, Z. Dong, and W. Zhu, Adv. Mater. **26**, 7185 (2014).
[47] J. Kang, W. Liu, D. Sarkar, D. Jena, and K. Banerjee, Phys. Rev. X **4**, 031005 (2014).
[48] V. M. Pereira, A. H. Castro Neto, and N. M. R. Peres, Phys. Rev. B **80**, 045401 (2009).
[49] C. Si, Z. Sun, and F. Liu, Nanoscale **8**, 3207 (2016).
[50] Y. Shi, W. Zhou, A.-Y. Lu, W. Fang, Y.-H. Lee, A. L. Hsu, S. M. Kim, K. K. Kim, H. Y. Yang, L.-J. Li *et al.*, Nano Lett. **12**, 2784 (2012).
[51] D. Pierucci, H. Henck, J. Avila, A. Balan, C. H. Naylor, G. Patriarche, Y. J. Dappe, M. G. Silly, F. Sirotti, A. C. Johnson *et al.*, Nano Lett. **16**, 4054 (2016).